New global observations of the terrestrial carbon cycle from GOSAT: Patterns of plant fluorescence with gross primary productivity

Christian Frankenberg,[1] Joshua B. Fisher,[1] John Worden,[1] Grayson Badgley,[1] Sassan S. Saatchi,[1] Jung-Eun Lee,[1] Geoffrey C. Toon,[1] André Butz,[2] Martin Jung,[3] Akihiko Kuze,[4] and Tatsuya Yokota[5]

[1] Our ability to close the Earth's carbon budget and predict feedbacks in a warming climate depends critically on knowing where, when and how carbon dioxide is exchanged between the land and atmosphere. Terrestrial gross primary production (GPP) constitutes the largest flux component in the global carbon budget, however significant uncertainties remain in GPP estimates and its seasonality. Empirically, we show that global spaceborne observations of solar induced chlorophyll fluorescence – occurring during photosynthesis – exhibit a strong linear correlation with GPP. We found that the fluorescence emission even without any additional climatic or model information has the same or better predictive skill in estimating GPP as those derived from traditional remotely-sensed vegetation indices using ancillary data and model assumptions. In boreal summer the generally strong linear correlation between fluorescence and GPP models weakens, attributable to discrepancies in savannas/croplands (18–48% higher fluorescence-based GPP derived by simple linear scaling), and high-latitude needleleaf forests (28–32% lower fluorescence). Our results demonstrate that retrievals of chlorophyll fluorescence provide direct global observational constraints for GPP and open an entirely new viewpoint on the global carbon cycle. We anticipate that global fluorescence data in combination with consolidated plant physiological fluorescence models will be a step-change in carbon cycle research and enable an unprecedented robustness in the understanding of the current and future carbon cycle. **Citation:** Frankenberg, C., et al. (2011), New global observations of the terrestrial carbon cycle from GOSAT: Patterns of plant fluorescence with gross primary productivity, *Geophys. Res. Lett.*, *38*, L17706, doi:10.1029/2011GL048738.

[2] Gross primary production (GPP) through photosynthesis by terrestrial ecosystems constitutes the largest global land carbon flux [*Zhao and Running*, 2010; *Beer et al.*, 2010]. Currently there are two main spatially explicit approaches to quantify GPP globally: 1) meteorology-driven full land surface carbon cycle models [*Friedlingstein et al.*, 2006; *Sitch et al.*, 2008]; and, 2) remote sensing-driven [*Zhao and Running*, 2010] and/or flux tower based [*Beer et al.*, 2010; *Jung et al.*, 2011] semi-empirical models focused on GPP or net primary production (NPP). Significant uncertainties related with the first approach are due to differing model sensitivities to meteorological parameters and uncertain global meteorological data sets [*Friedlingstein et al.*, 2006; *Sitch et al.*, 2008]. Uncertainties with the second approach exist because GPP cannot directly be estimated from the remote sensing measurements but is also modeled as a function of leaf area index (LAI) and fraction of absorbed photosynthetically active radiation (fAPAR) or greenness indices such as the normalized difference or enhanced vegetation indices (NDVI, EVI) [*Zhao et al.*, 2005]. These indices are often contaminated by atmospheric interference, and may contribute a misleading signal when vegetation becomes stressed, e.g., green canopies that are not photosynthesizing [*Huete et al.*, 2002].

[3] Remote sensing of solar-induced chlorophyll fluorescence (F_s) [*Krause and Weis*, 1991], as intended with the FLEX satellite mission, offers a direct physiology-based measure of global photosynthetic activity. Absorbed photosynthetically active radiation (APAR) within 400–700 nm wavelengths drives photosynthesis, but can also be dissipated into heat or re-radiated at longer wavelengths (660–800 nm), which is termed fluorescence. At the laboratory and field scale, chlorophyll fluorescence has been intensively studied [*Moya et al.*, 2004; *Corp et al.*, 2006; *Baker*, 2008; *Campbell et al.*, 2008; *Genty et al.*, 1989] but spaceborne remote sensing of fluorescence is more difficult [*Frankenberg et al.*, 2011] and accurate data has so far not been available. Concerning solar-induced steady state fluorescence, an implicit direct correlation with GPP exists as both depend on absorbed radiation. Also, field studies [*Flexas et al.*, 2002; *Damm et al.*, 2010; *Rascher et al.*, 2009] as well as theoretical modelling [*Van der Tol et al.*, 2009] show a clear positive correlation of CO_2 assimilation and stomatal conductance with F_s, especially because increases in heat dissipation under high light conditions cause a concurrent reduction of both fluorescence and photosynthesis yield. These physiological signals provided by fluorescence are not directly achievable with traditional vegetation remote sensing products, which model GPP using a multitude of ancillary data and model assumptions, all of which are prone to errors. Especially light use efficiency (LUE) is difficult to model on a global scale as it

[1]Jet Propulsion Laboratory, California Institute of Technology, Pasadena, California, USA.
[2]Karlsruhe Institute of Technology, Institute for Meteorology and Climate Research, Leopoldshafen, Germany.
[3]Biogeochemical Model-Data Integration Group, Max Planck Institute for Biogeochemistry, Jena, Germany.
[4]Japan Aerospace Exploration Agency, Tsukuba, Japan.
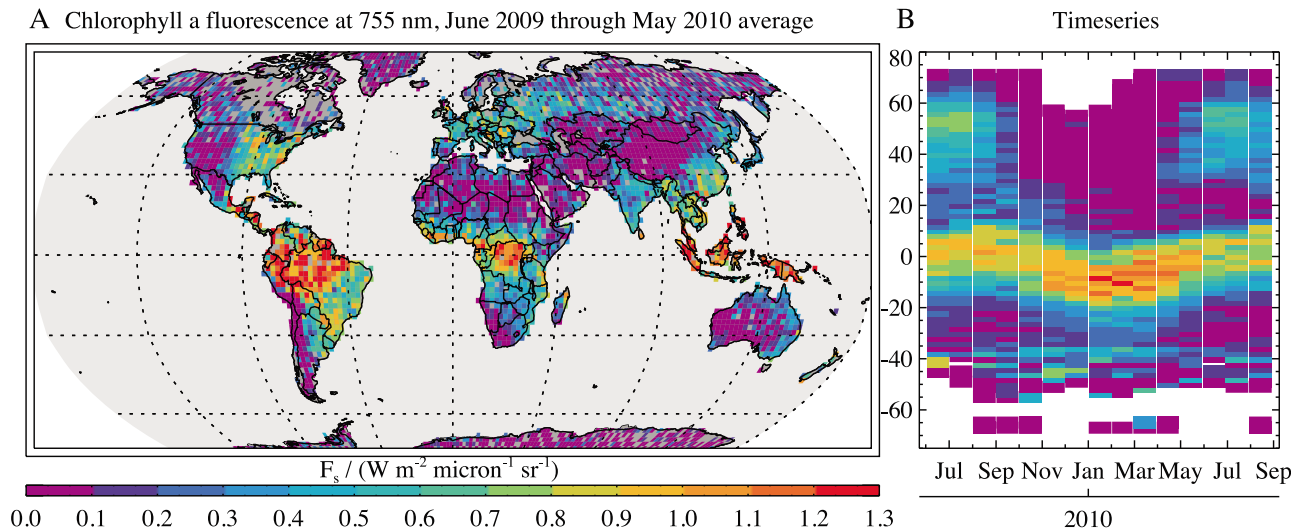[5]National Institute for Environmental Studies, Tsukuba, Japan.

A Chlorophyll a fluorescence at 755 nm, June 2009 through May 2010 average   B   Timeseries

Figure 1. (a) Annual average (June 2009 through May 2010) of retrieved chlorophyll-a fluorescence at 755 nm on a $2° × 2°$ grid. Only grid-boxes with more than 15 soundings constituting the average are displayed. (b) Latitudinal monthly averages of chlorophyll fluorescence from June 2009 through end of August 2010.

varies widely across biomes [*Turner et al.*, 2003] and depends on uncertain variables such as nutrient and water availability.

[4] As previously demonstrated [*Frankenberg et al.*, 2011; *Joiner et al.*, 2011], the fluorescence signal can be measured from space using high resolution spectra covering Fraunhofer lines (narrow absorption features in the solar spectrum) in the 660–800 nm range. By measuring the fractional depth of these lines, F_s can be accurately estimated, independent of scattering and albedo effects [*Frankenberg et al.*, 2011]. For the retrieval of steady-state solar induced chlorophyll fluorescence, we use radiance spectra measured in the red spectral range between 756–759 nm and also 770.5–774.5 nm, recorded by the TANSO Fourier Transform Spectrometer (FTS) on board the Japanese GOSAT satellite [*Hamazaki et al.*, 2005; *Kuze et al.*, 2009], which was launched on 23 January 2009 into a sun-synchronous orbit with a local overpass time of 13:00. ≈10000 soundings with 82 km^2 circular spatial footprints are recorded daily, repeating a regularly spaced global footprint grid every 3 days. We retrieved the solar-induced fluorescence signal F_s using an iterative least squares fitting technique. A unique and critical step in our data processing is the correction of an observed zero-level offset in acquired GOSAT O_2 A-band spectra. Without correction, the offset strongly biases F_s because its impact on Fraunhofer line depth is indistinguishable from fluorescence [*Frankenberg et al.*, 2011]. The bias in F_s, which can be higher than 100%, is positively correlated with radiance levels in the O_2 A-band. Therefore, the bias is large at low solar zenith angles and over bright surfaces (e.g., over tropical forest, ice and snow), in turn strongly impacting previous [*Joiner et al.*, 2011] analyses of GOSAT data.

[5] After correction, the annual average of F_s clearly reveals the contrast between highly active vegetation and barren or snow-covered surfaces (Figure 1a). Fluorescence maxima appear over tropical evergreen forests as well as the eastern United States followed by Asia and central Europe. Overall, the global map of chlorophyll fluorescence also

captures many small-scale features such as enhanced signal in southeastern Australia or the comparatively low values of the Iberian Peninsula. The temporal evolution of fluorescence is of particular interest because the seasonal variation of atmospheric carbon dioxide is dominated by the seasonality of GPP and respiration. We observe a pronounced seasonal cycle in the northern hemisphere as well as seasonal shifts in the location of maximum fluorescence in the tropics (Figure 1b). The southern hemisphere, conversely, exhibits a far smaller seasonal variability.

[6] Currently, the large footprint size, high single-measurement noise as well as the sparse and infrequent spatial sampling of the GOSAT FTS only provides a coarse global picture after substantial averaging, which impedes both ground-based validation as well as regional studies. Hence, we rely on model or other remotely sensed data for comparison on the global scale. As a benchmark, we compare against the MPI-BGC GPP model product [*Beer et al.*, 2010; *Jung et al.*, 2011] because it is derived from direct eddy-covariance flux tower measurements of GPP and is thus considered close to the truth where the flux tower density is high. We also use MODIS-derived GPP, as well as NDVI, EVI and LAI indices, because these products have been widely used as a proxy for GPP [*Myneni et al.*, 2007; *Zhao and Running*, 2010]. Additionally, we compare against the CASA GPP monthly climatology model [*van der Werf et al.*, 2003]. For the comparison with GPP, we convert the measured instantaneous fluorescence to daily averages (see auxiliary material), denoted by $\overline{F_S}$, as GPP is an integrated measure of carbon fluxes per day.[1] When comparing with vegetation indices, we ratio F_s by normalized down-welling PAR (approximated by the cosine of the solar zenith angle (SZA) at the time of measurement).

[7] On the annual average, we find a strong linear spatial correlation between $\overline{F_S}$ with model-based GPP, most notably with MPI-BGC ($r^2 = 0.81$) followed by MODIS

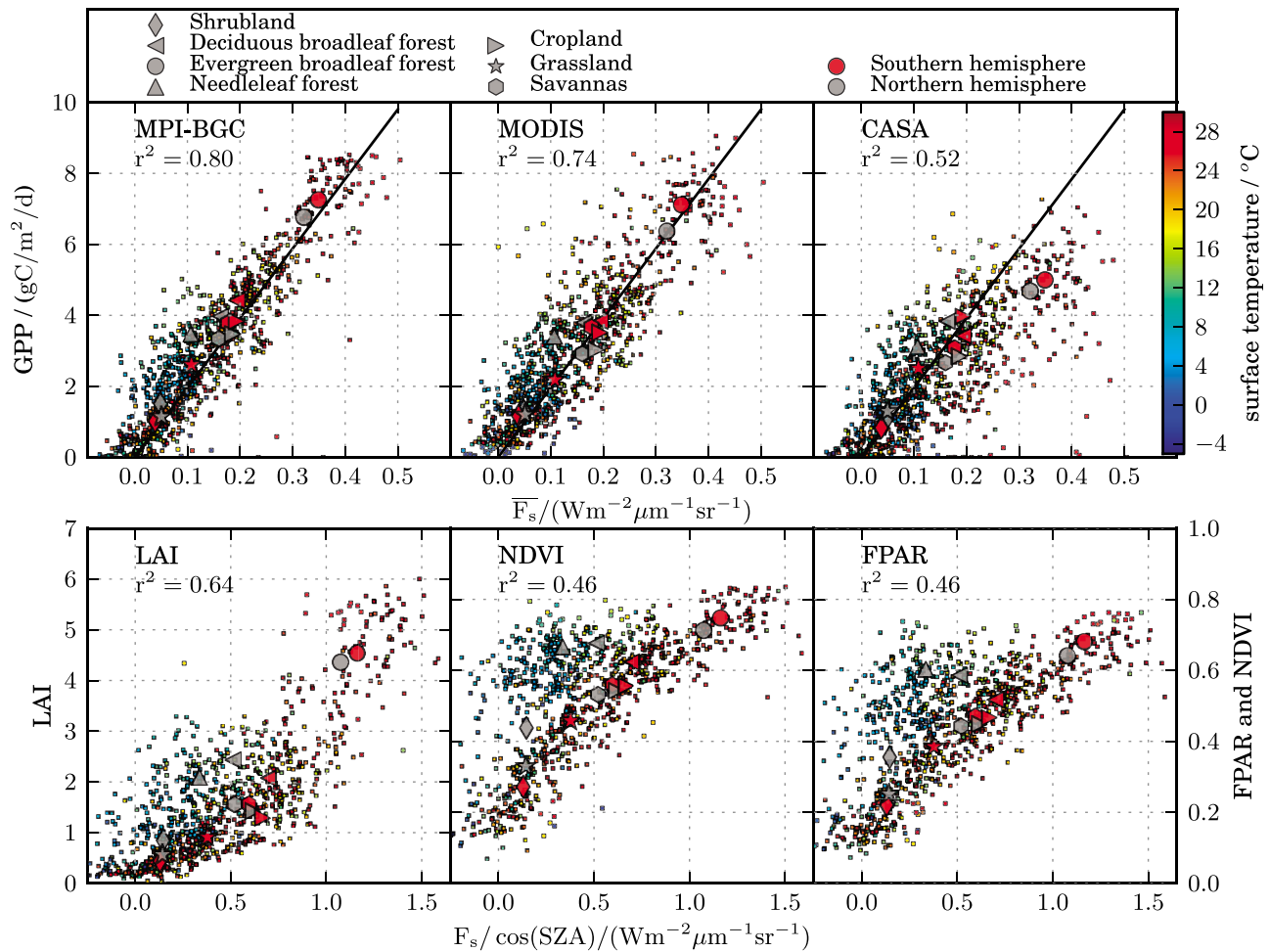[1]Auxiliary materials are available in the HTML. doi:10.1029/2011GL048738..

Figure 2. (top) Scatter-plot of $4° \times 4°$ grid cell averages of fluorescence ($\overline{F_S}$) vs. GPP model estimates (small dots color-coded by latitude, only grid boxes over vegetated areas and with a 1-σ precision error in $\overline{F_S}$ of <0.04 $Wm^{-2} \mu m^{-1} sr^{-1}$ are shown). The linear regression line in all panels equals a linear fit through the origin on the basis of the MPI-BGC GPP model. (bottom) Normalized F_s/cos(SZA) vs. MODIS LAI, NDVI and fPAR. The large symbols in all plots are biome averages, further separated for northern and southern hemisphere and based on $1 \times 1°$ biome classification see auxiliary material.

GPP ($r^2 = 0.74$), but significantly worse correlations against the other MODIS vegetation index products ($r^2 = 0.47$–0.63) and the CASA model ($r^2 = 0.52$) (Figure 2). Two biome types caused most of the differences in the comparisons: needleleaf forest for MPI-BGC and MODIS, and evergreen broadleaf forest for CASA. The MODIS greenness indices showed saturation at high values, particularly in high northern latitude needleleaf forests; this may be attributed to

problems with using greenness as an indicator for photosynthetic activity. This becomes evident in the correlation of vegetation indices with F_s, where the relationship appears curvilinear and needleleaf forests deviate most strongly regarding all indices, especially at low temperatures (Figure 2). Calculation of GPP from vegetation indices thus requires ancillary information, which can add further uncertainties. It is important to note that the chlorophyll

Table 1. Linear Pearson Correlation Coefficients (r^2) With Chlorophyll Fluorescence on $4° \times 4°$ Grid Cells for the Annual Average and Different Seasons[a]

Season	MPI-BGC GPP	MODIS GPP	CASA GPP	MODIS LAI	MODIS NDVI	MODIS fPAR	MODIS MPI GPP	CASA MPI GPP
JJA	0.76	0.56	0.57	0.53	0.48	0.44	0.82	0.74
SON	0.86	0.78	0.64	0.73	0.64	0.63	0.87	0.80
DJF	0.88	0.76	0.77	0.63	0.63	0.61	0.87	0.80
MAM	0.81	0.72	0.64	0.63	0.51	0.53	0.86	0.77
Annual	0.80	0.74	0.52	0.64	0.46	0.46	0.81	0.63
JJA-DJF	0.89	0.65	0.72	0.70	0.53	0.80	0.78	0.86

[a]Seasons: June-August 2009 (JJA), September-November 2009 (SON), December-February 2009–2010 (DJF) and March-May 2010 (MAM). Vegetation-free areas are excluded in the analysis. In addition, the correlation of the difference between JJA and DJF is displayed (JJA-DJF, see Figure S12 in Text S1). The two right columns indicate the correlation coefficients of MODIS against MPI-BGC and CASA against MPI-BGC, respectively.
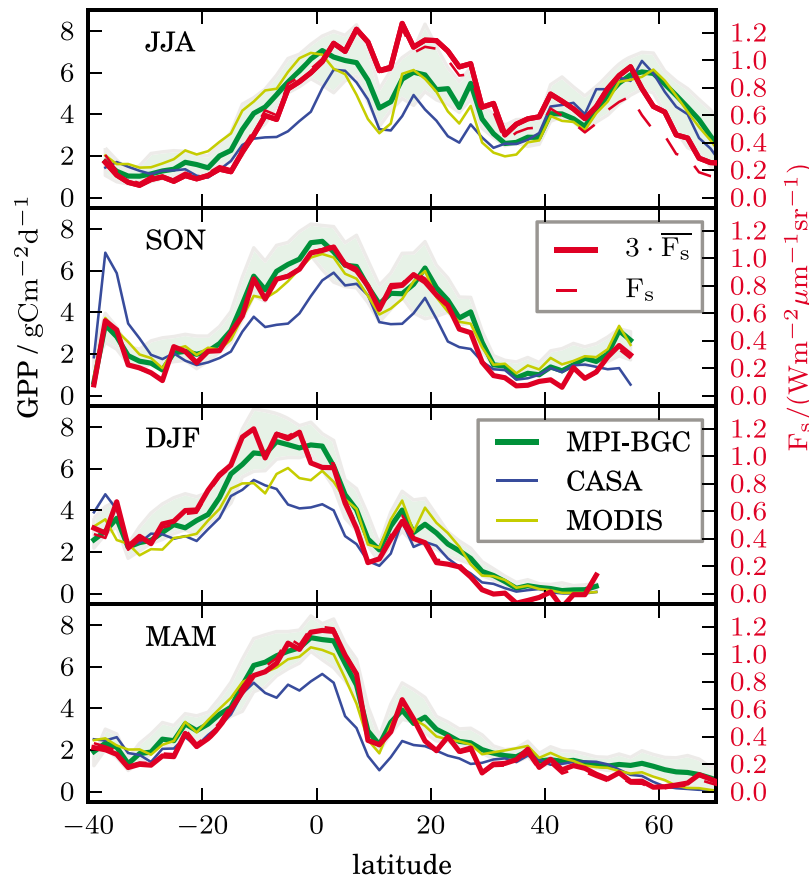
Figure 3. Latitudinal cross sections of fluorescence (F_s) and model GPP estimates for different seasons. The different y-axes are scaled according to the slope of the linear regression line as displayed in Figure 2 (i.e., fluorescence signals are directly comparable to GPP under the assumption of the linear correlation). The green-shaded area represents the ensemble range of the MPI-BGC GPP estimate [*Beer et al.*, 2010; *Jung et al.*, 2011].

fluorescence emission is the only dataset not sharing any information with all other datasets used here. In comparison with CASA, evergreen broadleaf forests are consistently low-biased against all other measurements, probably because LUE in CASA is only a function of climatic parameters [*Potter et al.*, 1993].

[8] Goodness of fit with the comparison products is not consistent seasonally. High r^2 with MPI-BGC GPP is observed in boreal autumn (SON) and winter (DJF) but is largely reduced in boreal summer (JJA) in all models (Table 1), most notably for MODIS and CASA GPP. Correlation of the raw fluorescence signal with MPI-BGC is as good as MODIS GPP with MPI-BGC, even though no interpretative model has yet been applied to the fluorescence data. For the seasonal amplitude (difference JJA-DJF), the correlation is significantly greater ($r^2 = 0.89$) than for MODIS GPP ($r^2 = 0.78$), which underestimates the seasonal variability especially in the southern hemisphere (see also Figure S12 in Text S1). The seasonal variability in GPP is of prime interest because a) systematic seasonal biases in models or vegetation indices may cancel out in the annual mean [*Turner et al.*, 2006] and b) seasonal variability in GPP largely determines the seasonal cycle of atmospheric CO_2 abundances. For all seasons, correlation is best with MPI-BGC GPP, underlining that chlorophyll fluorescence provides direct constraints on the timing and amplitude of GPP.

[9] With the exception of CASA, the latitudinal cross sections of fluorescence and model GPP, especially with MPI-BGC, agree well in almost all seasons (Figure 3). The fluorescence latitudinal distribution and change in time are mostly within the uncertainty range of MPI-BGC, with two notable exceptions during JJA, causing the correlation deterioration. First, the fluorescence is elevated between 10–40°N. Second, the fluorescence signal in the northern-most latitudes from 55–70°N is much lower, exhibiting a decline further south than the models. The discrepancy at 10–40°N is mostly due to African savannas and croplands in Asia which constitute 38% of total global GPP [*Beer et al.*, 2010] (fluorescence 18–48% higher than expected, see Figures S11, S14, and S15 in Text S1). High-latitude needleleaf forests (55–70°N), on the other hand, exhibit a 30% lower than expected fluorescence signal. We hypothesize that differences in fluorescence yield and light-use efficiency, potentially caused by water or nutrient limitation may be the reason for the discrepancy (see also auxiliary material, Figure S15 in Text S1). At high latitudes under low light conditions, deviations in the response of fluorescence as a function of GPP may also play a role as fluorescence and photosynthesis can compete under those circumstances [*Van der Tol et al.*, 2009]. However, at 10–40°N in boreal summer, high light conditions prevail and a stricter correlation of GPP with fluorescence is expected (but a deviation from the linear correlation cannot

yet be excluded with certainty). Savannas are difficult to model from meteorological observations because savanna vegetation imposes relatively more biological control over fluxes, and is less controlled by meteorological variability than are wetter ecosystems [*Baldocchi and Xu*, 2007]. Croplands are difficult to model on a global scale because of large variability in LUE, as well as uncertain irrigation and fertilization practices. Hence, ancillary data needed to derive GPP from vegetation indices may be biased. For MODIS GPP summer biases in needleleaf forests (positive) and croplands (negative) have also been observed in site-level evaluations and attributed to errors in LUE and an over-sensitive parameterization of vapor pressure deficit dependency [*Turner et al.*, 2005]. Further, the area with highest deviations is almost devoid of flux towers, increasing uncertainties in MPI-BGC. Even though the discrepancies cannot yet be unequivocally resolved, our results point to underestimations of light use efficiency for savannas and croplands in boreal summer (Figure S15 in Text S1).

[10] We acknowledge that the observed linear relationship is empirical and further studies are needed regarding the exact quantitative relationship of steady-state fluorescence [*Maxwell and Johnson*, 2000] with GPP under various light and temperature conditions and especially considering spatial scales largely exceeding leaf-level and laboratory scales. Eventually, this will unleash the full potential of global space-borne observations of fluorescence. However, we demonstrated the utility and simplicity of using raw fluorescence without any ancillary datasets or model assumptions as a direct linear predictor of GPP at the global scale. Moreover, the GOSAT satellite samples only once per day, does not cover the entire earth and was not even intended to retrieve fluorescence. Nevertheless, it can be anticipated that chlorophyll fluorescence retrievals from GOSAT and OCO-2 (taking about 50 times more data than GOSAT, hence largely reducing the uncertainty) in conjunction with their global atmospheric CO_2 measurements will provide an exceptional combination of a vegetation and atmospheric perspective on the global carbon budget, constraining our model predictions for future atmospheric CO_2 abundances.

References

Baker, N. (2008), Chlorophyll fluorescence: A probe of photosynthesis in vivo, *Annu. Rev. Plant Biol.*, *59*(1), 89–113.
Baldocchi, D., and L. Xu (2007), What limits evaporation from Mediterranean oak woodlands—The supply of moisture in the soil, physiological control by plants or the demand by the atmosphere?, *Adv. Water Resour.*, *30*(10), 2113–2122.
Beer, C., et al. (2010), Terrestrial gross carbon dioxide uptake: Global distribution and covariation with climate, *Science*, *329*(5993), 834–838.
Campbell, P., et al. (2008), Contribution of chlorophyll fluorescence to the apparent vegetation reflectance, *Sci. Total Environ.*, *404*(2–3), 433–439.
Corp, L., E. Middleton, J. McMurtrey, P. Entcheva Campbell, and L. Butcher (2006), Fluorescence sensing techniques for vegetation assessment, *Appl. Opt.*, *45*(5), 1023–1033.
Damm, A., et al. (2010), Remote sensing of sun-induced fluorescence to improve modeling of diurnal courses of gross primary production (GPP), *Global Change Biol.*, *16*(1), 171–186.
Flexas, J., J. Escalona, S. Evain, J. Gulías, I. Moya, C. Osmond, and H. Medrano (2002), Steady-state chlorophyll fluorescence (Fs) measurements as a tool to follow variations of net CO_2 assimilation and stomatal conductance during water-stress in C_3 plants, *Physiol. Plant.*, *114*(2), 231–240.
Frankenberg, C., A. Butz, and G. C. Toon (2011), Disentangling chlorophyll fluorescence from atmospheric scattering effects in O_2 A-band spectra of reflected sun-light, *Geophys. Res. Lett.*, *38*, L03801, doi:10.1029/2010GL045896.
Friedlingstein, P., et al. (2006), Climate-carbon cycle feedback analysis: Results from the C4MIP model intercomparison, *J. Clim.*, *19*(14), 3337–3353.
Genty, B., J. Briantais, and N. Baker (1989), The relationship between the quantum yield of photosynthetic electron transport and quenching of chlorophyll fluorescence, *Biochim. Biophys. Acta*, *990*(1), 87–92.
Hamazaki, T., Y. Kaneko, A. Kuze, and K. Kondo (2005), Fourier transform spectrometer for greenhouse gases observing satellite (GOSAT), *Proc. SPIE*, *5659*, 73, doi:10.1117/12.581198.
Huete, A., K. Didan, T. Miura, E. Rodriguez, X. Gao, and L. Ferreira (2002), Overview of the radiometric and biophysical performance of the modis vegetation indices, *Remote Sens. Environ.*, *83*(1–2), 195–213.
Joiner, J., Y. Yoshida, A. P. Vasilkov, Y. Yoshida, L. A. Corp, and E. M. Middleton (2011), First observations of global and seasonal terrestrial chlorophyll fluorescence from space, *Biogeosciences*, *8*(3), 637–651, doi:10.5194/bg-8-637-2011.
Jung, M., et al. (2011), Global patterns of land-atmosphere fluxes of carbon dioxide, latent heat, and sensible heat derived from eddy covariance, satellite, and meteorological observations, *J. Geophys. Res.*, doi:10.1029/2010JG001566, in press.
Krause, G., and E. Weis (1991), Chlorophyll fluorescence and photosynthesis: The basics, *Annu. Rev. Plant Biol.*, *42*(1), 313–349.
Kuze, A., H. Suto, M. Nakajima, and T. Hamazaki (2009), Thermal and near infrared sensor for carbon observation Fourier-transform spectrometer on the Greenhouse Gases Observing Satellite for greenhouse gases monitoring, *Appl. Opt.*, *48*(35), 6716–6733.
Maxwell, K., and G. Johnson (2000), Chlorophyll fluorescence—A practical guide, *J. Exp. Bot.*, *51*(345), 659–668.
Moya, I., L. Camenen, S. Evain, Y. Goulas, Z. Cerovic, G. Latouche, J. Flexas, and A. Ounis (2004), A new instrument for passive remote sensing: 1. measurements of sunlight-induced chlorophyll fluorescence, *Remote Sens. Environ.*, *91*(2), 186–197.
Myneni, R., et al. (2007), Large seasonal swings in leaf area of Amazon rainforests, *Proc. Natl. Acad. Sci. U. S. A.*, *104*(12), 4820–4823.
Potter, C. S., J. T. Randerson, C. B. Field, P. A. Matson, P. M. Vitousek, H. A. Mooney, and S. A. Klooster (1993), Terrestrial ecosystem production: A process model based on global satellite and surface data, *Global Biogeochem. Cycles*, *7*(4), 811–841.
Rascher, U., G. Agati, L. Alonso, G. Cecchi, S. Champagne, R. Colombo, A. Damm, F. Daumard, and E. Miguel (2009), CEFLES 2: The remote sensing component to quantify photosynthetic efficiency from the leaf to the region by measuring sun-induced fluorescence in the oxygen absorption bands, *Biogeosciences*, *6*(7), 1181–1198.
Sitch, S., et al. (2008), Evaluation of the terrestrial carbon cycle, future plant geography and climate-carbon cycle feedbacks using five dynamic global vegetation models (DGVMS), *Global Change Biol.*, *14*(9), 2015–2039.
Turner, D., S. Urbanski, D. Bremer, S. Wofsy, T. Meyers, S. Gower, and M. Gregory (2003), A cross-biome comparison of daily light use efficiency for gross primary production, *Global Change Biol.*, *9*(3), 383–395.
Turner, D., et al. (2005), Site-level evaluation of satellite-based global terrestrial gross primary production and net primary production monitoring, *Global Change Biol.*, *11*(4), 666–684.
Turner, D., et al. (2006), Evaluation of MODIS NPP and GPP products across multiple biomes, *Remote Sens. Environ.*, *102*(3–4), 282–292.
Van der Tol, C., W. Verhoef, and A. Rosema (2009), A model for chlorophyll fluorescence and photosynthesis at leaf scale, *Agric. For. Meteorol.*, *149*(1), 96–105.
van der Werf, G., J. Randerson, G. Collatz, and L. Giglio (2003), Carbon emissions from fires in tropical and subtropical ecosystems, *Global Change Biol.*, *9*(4), 547–562.
Zhao, M., and S. Running (2010), Drought-induced reduction in global terrestrial net primary production from 2000 through 2009, *Science*, *329*(5994), 940–943.

Zhao, M., F. Heinsch, R. Nemani, and S. Running (2005), Improvements of the modis terrestrial gross and net primary production global data set, *Remote Sens. Environ.*, 95(2), 164–176.

G. Badgley, J. B. Fisher, C. Frankenberg, J.-E. Lee, S. S. Saatchi, G. C. Toon, and J. Worden, Jet Propulsion Laboratory, California Institute of Technology, 4800 Oak Grove Dr., Pasadena, CA 91109, USA. (christian.frankenberg@jpl.nasa.gov)

A. Butz, Karlsruhe Institute of Technology, Institute for Meteorology and Climate Research, H.-v.-Helmholtz-Platz 1, D-76344 Leopoldshafen, Germany.

M. Jung, Biogeochemical Model-Data Integration Group, Max Planck Institute for Biogeochemistry, Hans-Knöll-Str. 10, D-07745 Jena, Germany.

A. Kuze, Japan Aerospace Exploration Agency, 2-1-1 Sengen, Tsukuba, Ibaraki 305-8505, Japan.

T. Yokota, National Institute for Environmental Studies, 16-2 Onogawa, Tsukuba, Ibaraki 305-8506, Japan.